applied sciences

MDPI

Article

Failure Process of High-Loess-Filled-Slopes (HLFSs) during Precipitation under Different Mitigation Measures

Yi Zhu [1], Jianqi Zhuang [2,*] and Yong Zhao [2]

[1] School of Land Engineering, Chang'an University, Xi'an 710054, China; zhuyi529@chd.edu.cn
[2] School of Geological Engineering and Geomatics, Chang'an University, Xi'an 710054, China; 2023126114@chd.edu.cn
* Correspondence: jqzhuang@chd.ecu.cn; Tel.: +86-29-82339256

Abstract: The problems of gully and soil erosion caused by large-scale urban construction and agricultural development in China have become more and more serious in recent years. In an effort to solve this problem, a series of gully stabilization and highland protection projects have been carried out on the Loess Plateau, and this has resulted in a large number of high-loess-filled-slopes (HLFSs). Although these filled slopes uses several different mitigation measures, the HLFSs have been eroded and destroyed under the action of water. In order to study the influence of different mitigation measures on the stability of HLFSs and their failure process, this paper uses a flume test of the effects of various mitigation measures on this failure process. The results show that: (1) the failure processes of slopes with different mitigation measures are obviously different. Slope deformation u with a declining gradient mitigation mainly occurs on the surface of the slope body, and although slope erosion is quite serious, the slope does not fail as a whole. Slopes with a stepwise drainage channel mitigation show little erosion, but material can easily slide along the horizontal drainage channels. (2) The slope deformation process is correlated with changes in pore-water pressure. When local instability occurs, there is always a pre-process of continuously rising pore-water pressure. When a failure occurs, the pore-water pressure of the soil at each position of the slope body suddenly fluctuates under instantaneous excitation. (3) The response of soil pore pressure and the development characteristics of tension cracks affect the deformation of the slopes, which is also the cause of the differences slope instability caused by different mitigation measures. These research results provide reference for the protection of HLFS engineering projects from heavy rains.

Keywords: loess; high filled slope; failure process; mitigation measures; experimental

Citation: Zhu, Y.; Zhuang, J.; Zhao, Y. Failure Process of High-Loess-Filled-Slopes (HLFSs) during Precipitation under Different Mitigation Measures. *Appl. Sci.* **2024**, *14*, 419. https://doi.org/10.3390/app14010419

Academic Editor: Yosoon Choi

Received: 12 December 2023
Revised: 27 December 2023
Accepted: 29 December 2023
Published: 3 January 2024

1. Introduction

Loess soil covers about 10% of the Earth's land surface [1,2], and it covers the north-eastern, northwestern, and middle of the Yellow River regions in China. The total area of loess in China is estimated to be as much as 630,000 km^2, accounting for 6.63% of the total land area [2]. Loess soil supports one sixth of the Chinese population and constitutes one fifth of China's arable land area, with over 700 important towns and cities distributed within loess soil [3,4]. However, the loose structure of loess, the presence of numerous gullies on the surface of loess soil, and frequent rainstorms that cause severe erosion, make the region prone to frequent geohazards that pose a serious threat to engineering activities and the population in general [5–8]. Loess areas are densely covered with hills and gullies, and the surface has a fragmented terrain [9,10]. Therefore, many towns located in the Loess Plateau are constrained by limited space and geohazards, making further development difficult [11]. In recent years, various major projects have been carried out in the Loess Plateau to accelerate urbanization and improve the standards of living of residents [12–14], making it more critical than ever to understand how loess soil behaves under various engineering attempts to mitigate inevitable water erosion.

For example, in order to mitigate the issue of erosion in the loess tableland area in Qingyang City, Gansu Province, a major project called "Gully Stabilization and Tableland Protection" was carried out; the project that involved the burial of 14,035 gullies in 42 large tablelands within the city area. In Yan'an City, Shaanxi Province, and Lanzhou City, Gansu Province, the "Plain-to-Mountain Urban Construction" project was launched to accelerate urbanization and expand the scale of urban areas [10,12–14]. During the implementation of these projects, many high slopes were inevitably generated due to excavation and filling operations [10,12,13]. Consequently, these projects have resulted in various mitigation measures [15]. Although some slopes have merely been leveled without any protection, others have undergone drainage treatment. Nevertheless, the stability of such slopes remains uncertain, and the effectiveness of slope protection measures warrants evaluation. On-site field investigations have revealed severe erosion and damage to some slopes which with different protective measures (Figure 1). Hence, it is critical to study the stability of HLFSs under different protective measures, especially during rainfall. Accurate descriptions of the modes and mechanisms of slope instability, along with implementing corresponding geohazard prevention and mitigation measures, hold significant reference value for engineers [12,15].

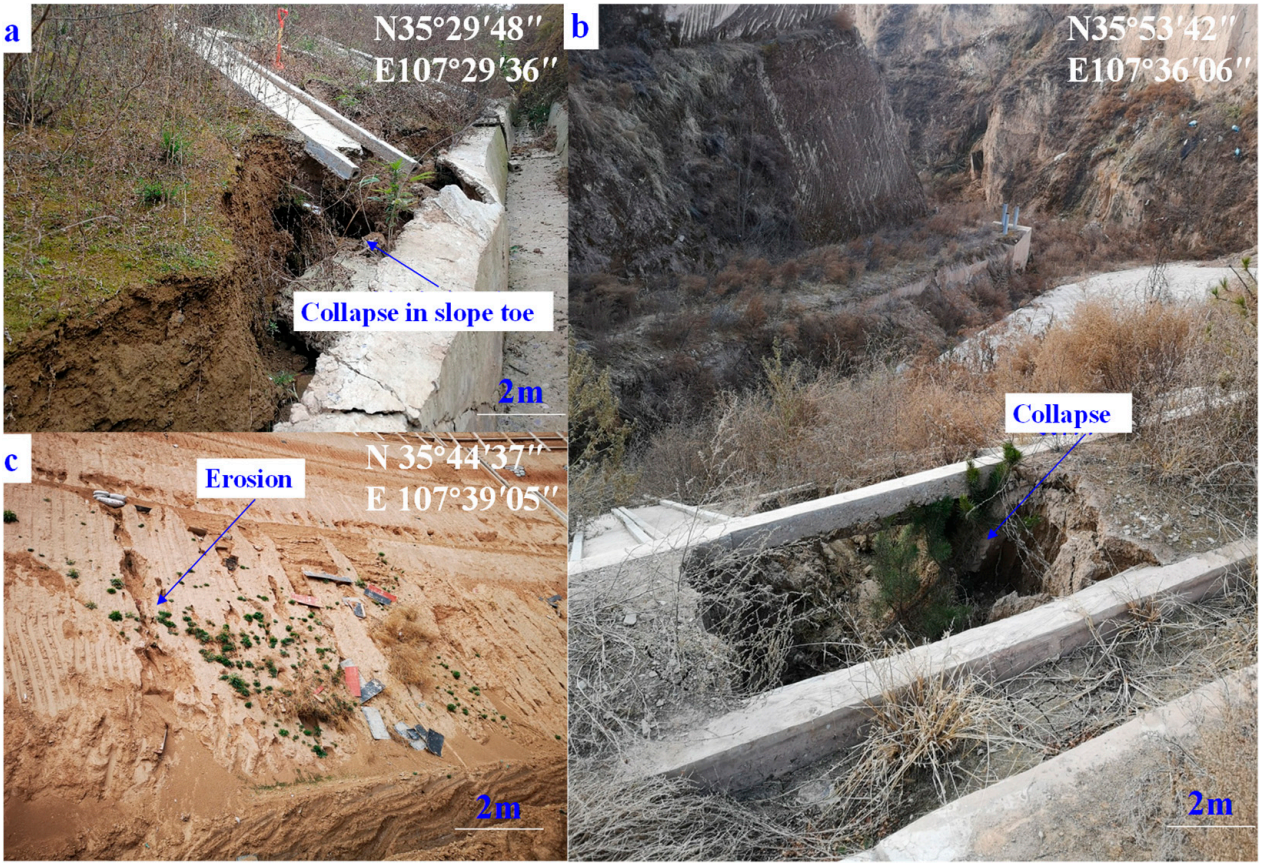

Figure 1. Erosion due to precipitation in the Gully Stabilization and Highland Protection projects ((**a**) collapse in the toe of the slope which with a stepwise drainage channel mitigation; (**b**) collapse on the slope which with a stepwise drainage channel mitigation; (**c**) erosion along the slope surface which with a declining gradient mitigation).

Extreme or prolonged periods of rainfall are the primary triggers of geohazards such as landslides and debris flows [11,16–18]. The rainfall and water infiltration process increases the moisture content of the soil, thereby reducing the soil's matrix suction and shear strength, ultimately leading to slope instability and deformation [19,20]. In the China's Loess Plateau, the unique loess landforms and the frequent occurrence of extreme rainfall

events have led to equally frequent geohazards [3,21–23]. Moreover, water infiltration is also a leading cause of slope instability and destruction in various engineering projects, as exemplified by reported cases such as the Guangming New District landslide in Shenzhen, the Lvliang Airport landslide, and the Bai Lu Yuan Baqiao landslide in Xi'an [24–27].

Indoor physical modeling experiments are commonly used for studying slope stability process and mechanism as they provide several advantages. One such advantage is the ability to create homogeneous soil slopes and control experimental conditions, ensuring that the results are not influenced by unknown factors [28–30]. Additionally, devices such as sensors can be utilized to monitor changes in micro-parameters during the simulation process [31]. Many researchers have conducted numerous studies on slope stability, instability, and failure processes using this method [32,33]. For example, Wu et al. [34] investigated the occurrence patterns and mechanisms of shallow landslides in loess under continuous heavy rainfall and intermittent heavy rainfall conditions through multiple sets of experimental comparisons. Likewise, Lin et al. [35] analyzed the influence of rainfall characteristics on the instability process of soil slopes by establishing a model under both low (40 mm/h) and high intensity (80 mm/h) rainfall conditions, and provided recommendations for selecting rainfall warning benchmark parameters. Furthermore, Rolando et al. [36] examined the instability process of slopes under sidewall seepage conditions and analyzed the slope instability mechanism using sensor data. Ten physical modeling experiments were also carried out to investigate the similarities and differences in slope instability and failure modes under various rainfall intensities ranging from low (18 mm/h) to high (63.5 mm/h) by Ahmadi-Adli et al. [37], and scholars have also replicated the initiation process of landslides, debris flows, and other geohazards by setting specific experimental conditions indoors [36]. For example, Hu et al. [38,39] reproduced the process of debris flow disasters caused by runoff in the Wenchuan earthquake zone through indoor modeling experiments and analyzed the initiating mechanism. Moreover, some scholars have studied the influence of specific factors on slope stability through comparative experiments, including soil initial moisture content [40], soil particle size distribution [39,41], and fine particle content [41].

This study is focused on the HLFS failure mode and process triggered by precipitation under different mitigation measures. We conducted indoor physical model experiments and analyzed the differences in failure modes and mechanisms using sensor data, 3D laser scanner data, and direct observations of the experimental phenomena, the results can provide a reference for optimization mitigation measures for the "Gully Stabilization and Tableland Protection".

2. Materials and Methods

2.1. Physical Characters of Materials

The loess sample used in our experiments was taken from the HLFS in Qingyang City, Gansu Province, and its particle size distribution of the soil sample was measured using a Bettersize 2000 laser particle size analyzer which made by Bettersize Instruments Ltd. of China. Particles with a size > 0.075 mm accounted for 15.2% of the sample, particles ranging from 0.075 mm to 0.005 mm accounted for 67.5%, and particles < 0.005 mm accounted for 17.3%, making it a typical fine loess soil. The plastic limit of the soil was 17.7%, the liquid limit was 38.63%, and the plasticity index was 20.93. The basic physical properties of the soil as obtained from geotechnical tests are shown in Table 1.

Table 1. The basic physical properties of the loess sample.

	Natural Water Content	Natural Dry Density	Plastic Limit	Fluid Limit	Plasticity Index	Particle Distribution (%)		
	w/(%)	ρ/(g·cm^{-3})	W_P/(%)	W_L/(%)	I_p/(%)	>0.075 mm	0.005–0.075 mm	<0.005 mm
Loess materials	12.2%	1.517	17.7	38.63	20.93	15.2	67.5	17.3

2.2. Test Flume

All experiments involved a flume model that consisted of three parts: an experimental slope system, a rainfall system, and a data acquisition system. The experimental slope system included a flume box and an experimental slope with dimensions of 2 m long, 0.6 m wide, and 1.2 m high, and the side of the box was made of tempered glass to allow for observation during the experiment. The bottom of the box was made of sealed waterproof wood to simulate an impermeable boundary (Figure 2), and the rainfall system consisted of a water supply tank, rainfall nozzles, and rain gauges. Distances between multiple rainfall nozzles were arranged according to specific calculations to ensure the uniformity of rainfall intensity in the flume. The data acquisition system included pore-water pressure sensors, water content sensors, displacement sensors, a 3D laser scanner, and a in particular, the pore-water pressure sensors and water content sensors were placed at different depths in the experimental slope to obtain the variations of the water content and pore-water pressure of the tested slope during the experiment. To monitor the displacement deformation of the slope, a displacement monitoring device that consisted of a hollow sphere with a diameter of 2 cm and a weight of 10 g buried 5 cm deep inside the slope and connected to the displacement sensor at the upper end via a steel wire with a diameter of 0.5 mm was set up inside the tested slope. A certain amount of counterweight was applied at the lower end of the sphere to ensure that the sphere was in a state of force balance in the initial state and to reduce the relative movement between the sphere and the surrounding soil [28]. Finally, the 3D scanner was placed directly in front of the flume box to collect the three-dimensional deformation data of the tested slope at different stages during the experiment.

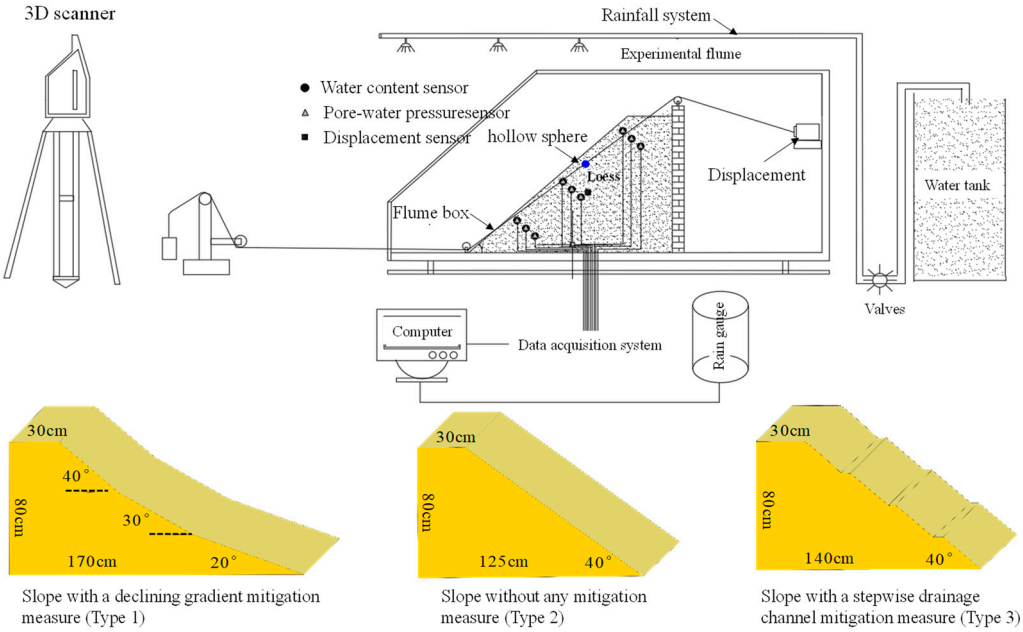

Figure 2. Schematic drawing of the experimental flume and slope type in the experimental.

2.3. Methods

During the test, constant rainfall intensity was used to simulate natural rainfall. According to the meteorological data of Qingyang City, the area is located in a monsoon climate zone, with frequent heavy rains during the rainy season. On 21 July 2019, the hourly precipitation in the Qingyang City even reached 90 mm. In order to present the local characteristics of heavy rainfall, the rainfall intensity of the test was set at 80 mm/h, and the slope in the experiment was set according to the actual slopes in the HLFSs in the "Gully Stabilization and Tableland Protection" in Qingyang, which were initially designed to be 40°. The experimental slope height of the test was 80 cm, and only the mitigation measures on the slope surface were modified with each trial. Soil samples were placed

layer-by-layer with 15 cm per layer and compacted multiple times to a dry density of 1.5 g/cm^3. Before placing a new layer of soil, the compacted surface of the underlying soil layer was ensured the uniformity of the slope and prevent interlayer sliding. When placing a soil sample, pore-water pressure and water content sensors were placed at the upper part of slope, middle part of slope, and toe of the slope as well, with vertical depths of 5 cm, 10 cm, and 15 cm from the slope surface, respectively. Before conducting each test, the test slope was allowed to settle until the sensor readings stabilized. The sensors recorded changes in soil content, pore-water pressure, and displacement at a sampling frequency of once per second, and the laser scanner conducted multiple real-time scans based on the shape changes in the test slope.

3. Results

3.1. Water Content Changes

The changes in the water content of different parts of the slopes with different types of mitigation measures are shown in Figure 3, and from the figure we can see that the changes were all quite similar. First, the water content gradually decreased before finally leveling off in all cases. In the early stage of testing, the infiltration rate of rainwater was relatively fast, and the soil water content curves increased rapidly within 15 min after the initial change in water content before stabilizing. In the later stage of the experiment, the slope surfaces reached saturation, and the water content of the soil at different positions and depths stayed at around 60%. In addition, the rainwater infiltration rates of all types of slopes showed were fastest at the upper part of the slope and became slower toward the toe.

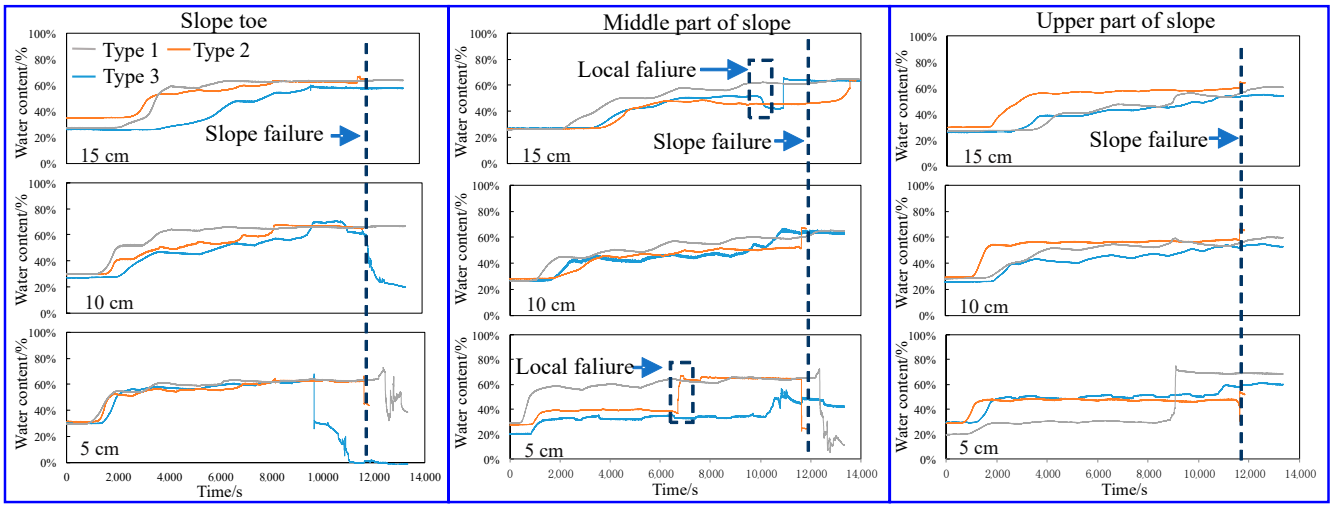

Figure 3. Water content changes for different slopes at different sites.

As far as what differences there were in the water content changes with different types of mitigation measures, due to the converging effect of the slope drainage channels, which effectively prevent rainwater from accumulating on the slope surface, the time until rainwater infiltration to deep soil (15 cm) was relatively slow (Figure 3). Additionally, the infiltration rate of slopes with a stepwise drainage channel mitigation measure was slower than with the other two types of slopes, and the time required for the soil to reach saturation was longer as well.

Regarding local changes, the water content changes in slopes without any mitigation measures were linked to both local and overall failure. When a large-scale block failure occurred at the slope middle, the moisture sensors (5 cm) had obvious fluctuations. The same phenomenon also occurred when the overall slope failed. From Figure 3 we can see that this change was synchronous with the instability of the slope and was a nearly instantaneous change. The response of shallow soil (5 cm) was the most obvious. Shallow

soil tends to become compacted during motion, so any soil water it holds is discharged, and its water content decreases sharply when this happens. Some of the water diffuses to deeper soil, so the water content of the deeper soil then rises slightly.

When the slope without any mitigation measures failed, the water content of the shallow soil (5 cm) at the upper, middle, and toe of the slope all showed almost instantaneous drops, with the most obvious changes at the upper and middle parts and only a slight change at the toes. The water content of the deeper soil (10 cm, 15 cm) also changed but varied within wide limits. These changes in water content did not appear in the other two types of slopes. The slope with the step-by-step mitigation measure had failures mainly concentrated on the slope surface, and a landslide even occurred in the later stage that had a relatively shallow depth little impact on the deeper soil's water content. Therefore, in the later stage of the experiment, the soil water content of the slope with a declining gradient mitigation did not undergo any sudden changes. The water content of the slope with a stepwise drainage channel mitigation measure also did not undergo any sudden changes, and the water content of the soil at each position increase gradually without sudden uplifts or drops.

3.2. Pore-Water Pressure Changes

Variations in pore-water pressure show a periodicity and strong correlation with the slope deformation [42,43]. In our experiments, fluctuations in pore-water pressure mainly occurred during various stages of slope failure. In the initial stage of the testing, the deformation of the slope occurred due to creep caused by an increase in the slope's water content and erosion on the slope surface. During this stage, the pore-water pressure at the toe and middle part of the slope changes only slightly, with a small upward trend (Figure 4).

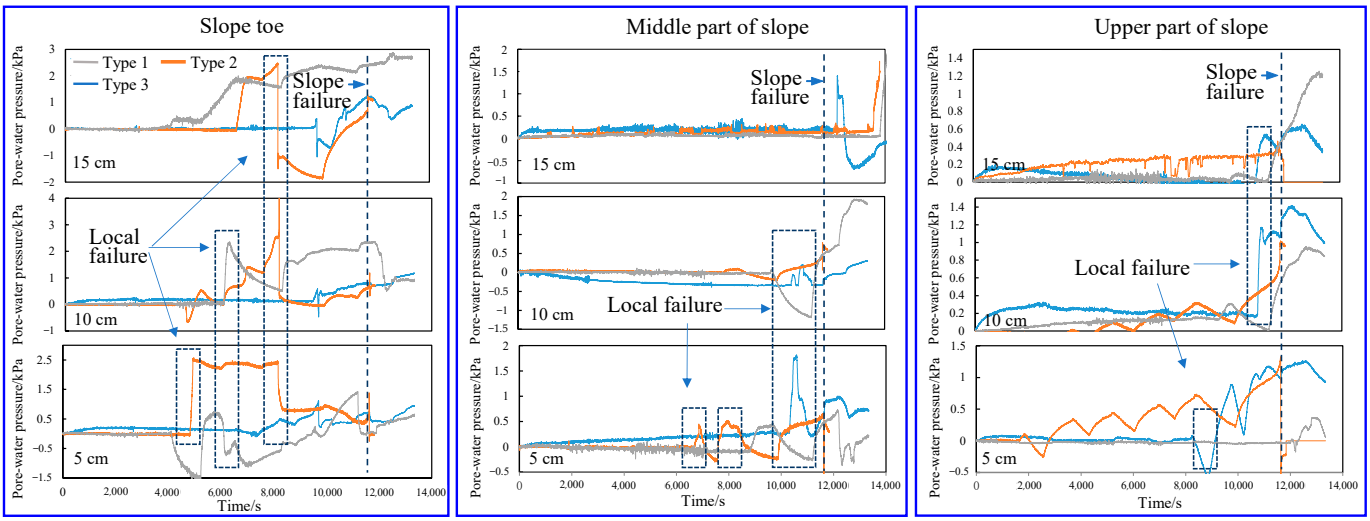

Figure 4. Pore-water pressure changes for different slopes at different sites.

In the second stage of the testing, continuous rainfall caused surface instability and a shallow slide in the slopes, and the pore-water pressure changed with these events (Figure 4). The pore-water pressure in given area had significant fluctuations during local failures in that area. When the sliding depth was shallow, only the surface pore-water pressure had significant changes, and when the sliding depth was high, the pore-water pressure at different depths had a significant response. The responses of pore-water pressure during local failure of slopes with different mitigation measures were slightly different, however (Figure 4). Specifically, the fluctuation of pore-water pressure on the slope without any mitigation measure mainly occurred in the shallow soil (5 cm), and the pore-water pressure variation in the deep soil did not change significantly. Combined with the deformation data, this indicates that when a local failure occurred, the pore-water

pressure was mainly concentrated in the soil 5–15 cm deep from the slope surface, which means that the failure depth was concentrated at 5–15 cm as well. In the slope with step-by-step mitigation, the change in pore-water pressure was not significant, which indicates that at this stage, the response of the slope to rainfall was mainly concentrated on the surface. Although the water content in the deep soil increased, the pore-water pressure did not increase significantly, and the failure was mainly in the shallow soil. In the slope with a stepwise drainage channel mitigation, the pore-water pressure changed more rapidly, and the pore-water pressure in the deep soil (15 cm) was larger than in the other two types of slopes, indicating that the sliding surface of the slope was deeper than the other two types of slopes as well.

In the last stage of the testing, the slope without any mitigation measures experienced overall failure along a sliding surface under continuous rainfall. Pore-water pressure at different depths and locations underwent rapid changes all at the same time as well. The most significant change in pore-water pressure occurred in the shallow soil, and the change in the deep soil was relatively small. Unlike the changes in the second stage, the change in pore-water pressure was nearly instantaneous. The trend in pore-water pressure changed at different positions and was a sudden increase within 1–2 s, followed by a rapid decrease prior to stabilization. This phenomenon is due to the rapid failure of the entire slope causing almost instant displacement of various parts of the slope and subsequent poor drainage that led to excess pore water pressure. This in turn caused a sudden increase in pore-water pressure in various parts of the slope [44–46]. The slope with a declining gradient mitigation also experienced shallow sliding, with a synchronous increase in pore-water pressure at all parts of the slope before eventually stabilizing.

Compared to the slope without any mitigation measures, the changes in pore-water pressure in the slope with a declining gradient mitigation were more gradual, with a clear process of continuous growth and no pore-water pressure surges. The amplitude of the pore-water pressure response for the slope with a stepwise drainage channel mitigation was the highest during the local failure stage, and the subsequent pore-water pressure fluctuations were relatively weaker than with the other two types of slopes. During both local and overall failures, pore-water pressure both increased and decreased. Pore-water pressure decreased and became negative at the upper and middle part of the slope but increased at the toe of the slope. This indicates that the toe of the slope exhibited shear contraction characteristics that led to a sharp increase in pore-water pressure and that the upper part of the slope exhibited a tension stress state that led to a sharp drop in pore-water pressure [45,46].

3.3. Deformation

Deformation is the most important external manifestation of slope failure, and the type and characteristics of slope deformation over time are the most effective means for early landslide warnings [42,43,47,48]. For the slope without any mitigation measures (Figure 5), after 6 min of rainfall, the water began to flow on the slope surface, and then the surface began to be eroded. In the first 60 min of continuous rainfall, the erosion at the toe of the slope gradually intensified. Erosion at various points at the toe of the slope gradually connected, and the toe of the slope kept retreating. The longest retreat distance was 28 cm, and small cracks appeared at the toe of the slope (Figure 5a). During 60–90 min of continuous rainfall, the toe of the slope continued to erode, and large blocks of the slope began to collapse. Erosion gullies longer than 10 cm were formed on the slope surface, and continuous deformation at the toe of the slope formed an upright lateral free face at the front edge of the slope. Tension cracks appeared at different heights on the upper and middle part of the slope as well (Figure 5b). During 90–140 min of rainfall, erosion at the toe of the slope continued, and cracks deepened and widened at the middle part of the slope, gradually connecting and penetrating each other. Large blocks of the slope collapsed along the cracks, and the longest retreat length of the slope surface reached 52 cm (Figure 5c).

After 193 min of rainfall, the entire slope failed and slid down with a slide depth of 10 cm and a slide distance of 52 cm (Figure 5d).

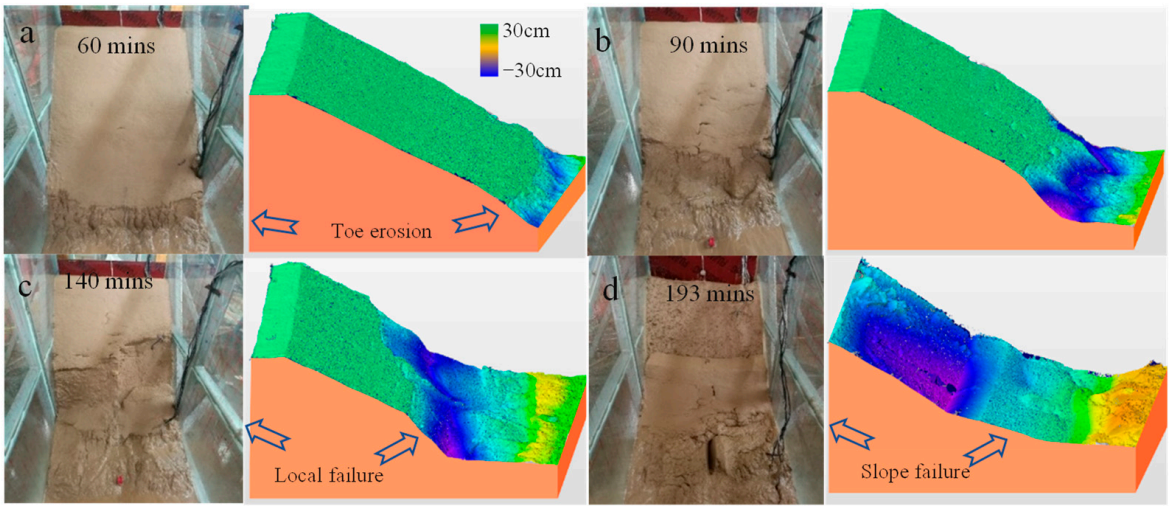

Figure 5. The process of failure for the slope without any mitigation measures ((**a**–**d**) are the 60 min, 90 min, 140 min and 193 min after experimental).

For the slope with a declining gradient mitigation (Figure 6), water began to flow on the slope surface after 5 min of rainfall, and local erosion was observed at the toe of the slope after 10 min. After 30 min of rainfall, erosion gullies at various points at the toe of the slope had connected and penetrated each other, and the toe edge of the slope kept retreating to a longest distance of 15 cm (Figure 6a). After 60 min of rainfall, the erosion continued at the toe of the slope, and the longest retreat distance was 28 cm. Tension cracks occurred in the lower part of the slope surface as well (Figure 6b). During 90–120 min of rainfall, tension cracks in the lower part of the slope surface deepened and widened, gradually connecting and penetrating each other. Local collapse occurred along the cracks at the toe of the slope (Figure 6c). After 150 min of rainfall, tension cracks appeared at all parts of the slope, and the cracks deepened and widened, eventually penetrating each other and forming multiple transverse cracks that penetrated the slope surface. After 180 min of rainfall, a shallow landslide with a depth of 5 cm occurred along the transverse cracks on the slope surface (Figure 6d), but the entire slope was still stable.

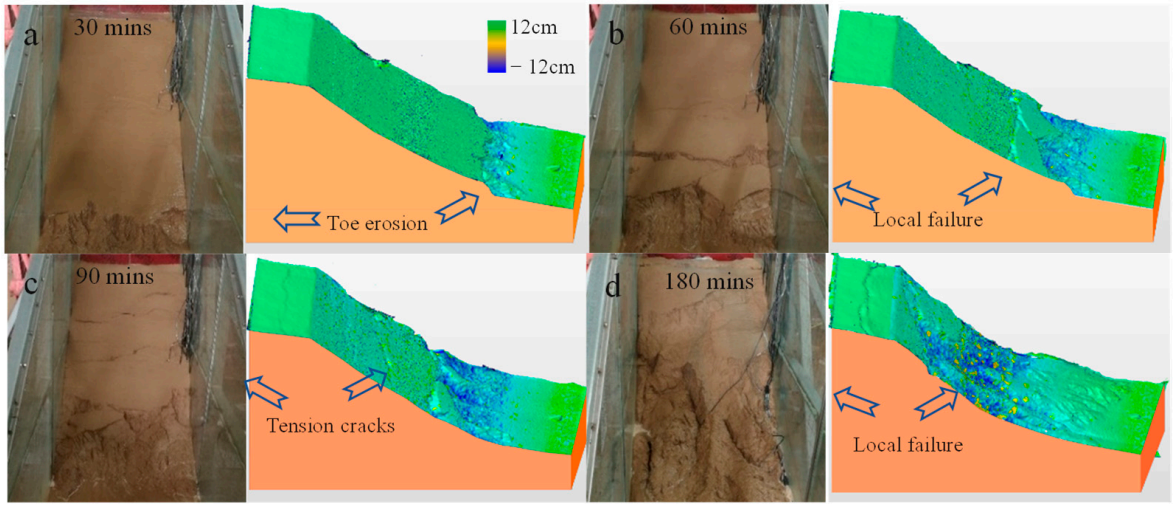

Figure 6. The process of failure for the slope with step-by-step mitigation ((**a**–**d**) are the 30 min, 60 min, 90 min and 180 min after experimental).

For the slope with a stepwise drainage channel mitigation (Figure 7), after 5 min of rainfall, water began to flow on the surface, and localized erosion was observed at the toe of the slope after 10 min. After 30 min of rainfall, settlement cracks gradually appeared and deepened near the toe of the slope, and after 40 min of rainfall, the failed locally, and some soil masses collapsed, producing a steep and high lateral free face at the toe of the slope (Figure 7a). After 60 min of rainfall, the toe of the slope was almost completely destroyed after multiple local failures, and the drainage channel at the toe of the slope was left hanging (Figure 7b). During rainfall of 90–120 min, multiple local failures occurred gradually upward along the transverse drainage channels on the slope, resulting in serious damage to the slope surface (Figure 7c). After 150 min of rainfall, local failures occurred in all parts of the slope, horizontal tensile cracks appeared at the upper part of the slope, and multiple steep lateral free faces appeared at the toe edge of the slope (Figure 7d). However, there was no overall instability.

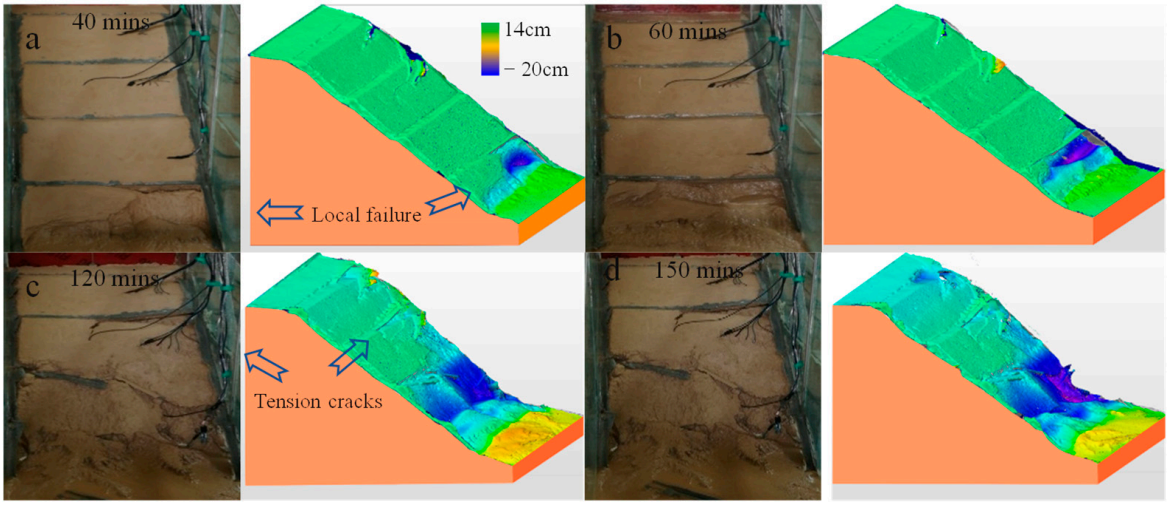

Figure 7. The process of failure for the slope with a stepwise drainage channel mitigation ((**a**–**d**) are the 40 min, 60 min, 120 min and 150 min after experimental).

3.4. A Model of the Failure Process

Based on the deformation characteristics and changes in the slopes during rainfall, the toes of the slopes were the first parts to fail, for all tested slopes, which initiated the failure process. During the failure process, slope erosion and local failures occurred for all tested slopes, but the failure modes of the slopes differed according to the mitigation measures. Based on the soil parameters and deformation processes of the tested slopes, the failure modes and differences of each slope can be described in the following stages.

(1) **Toe erosion.** After about 30 min of testing, slope surface soil gradually becomes saturated, and the infiltration rate of rainfall on the slope surface is lower than the rate of rainfall supply. The surface of the slope begins to accumulate water during this time, and slope erosion and local failures occur at the toe of the slope due to the continuous erosion of surface runoff and the softening effect of rainfall infiltration. Different mitigation measures showed different degrees of slope erosion and response times (as shown in Figure 8a). For the slope with a declining gradient mitigation, the slope erosion was more rapid and obvious due to its longer length, gentler gradient, and more obvious convergence flow. However, this gentler gradient also made it difficult for high and steep lateral faces to form at the toe of the slope. For the slope with a stepwise drainage channel mitigation, the effect of surface runoff was not obvious in the early stages of rainfall due to the collection effect of the slope drainage channel. Slope toe erosion and damage did not occur, and rainfall infiltration was slow. Therefore, there was no obvious deformation on the slope surface in the first 30 min. This was in stark contrast to the other two types of slopes where

obvious slope toe erosion occurred after only 10 min of rainfall. This also shows that constructing drainage channels on a slope can effectively reduce erosion due to rainfall and therefore slope damage.

(2) **Formation and expansion of slope surface cracks.** The slope body generates tensile stress towards the direction of the free surface and undergoes continuous creep due to slope toe erosion. In our experiments slope deformation accumulated gradually, and tensile cracks appeared on the slope surface in the vicinity of the free surface of the slope toe. However, the crack evolution patterns differed between different slopes (Figure 8b). For the slope without any mitigation measures, the appearance of tensile cracks occurred in an obvious sequence. For the slope with a declining gradient mitigation, the tensile cracks appeared simultaneously at various positions on the slope surface, without an obvious sequence. For the slope with a stepwise drainage channel mitigation, the tensile cracks all appeared near the transverse drainage channels on the slope surface.

(3) **Local failure.** The expansion of cracks causes the local pore-water pressure to increase continuously, and the effective stress of the soil decreases. Connected cracks form a potential sliding surface, and the local failures occur along the cracks. The location and magnitude of local failures in our testing were affected by slope mitigation measures (Figure 8c). In particular, the local failure in the slope with a declining gradient mitigation was small, and mainly occurred in the soil layer no deeper than 5 cm. The local failure in the slope with a stepwise drainage channel mitigation was larger, and the sliding surface was deeper. However, the overall deformation was smaller, and the collapse only occurred at the toe of the slope.

(4) **Overall failure.** Continuous local failures cause the free surface of the toe of the slope to become steeper, and the tensile stress on the slope increases continuously. The cumulative displacement of the slope body accelerates and gradually reaches its critical displacement. Immediately after this the potential sliding surface of the slope is penetrated, resulting in the overall failure of the slope. According to our tests, the slope without any mitigation measures experienced overall failure under continuous heavy rainfall, but the other two types of slopes did not exhibit overall failure. These slopes with mitigation measures only exhibited local failure at the slope toe and local failure due to shallow erosion sliding (Figure 8d).

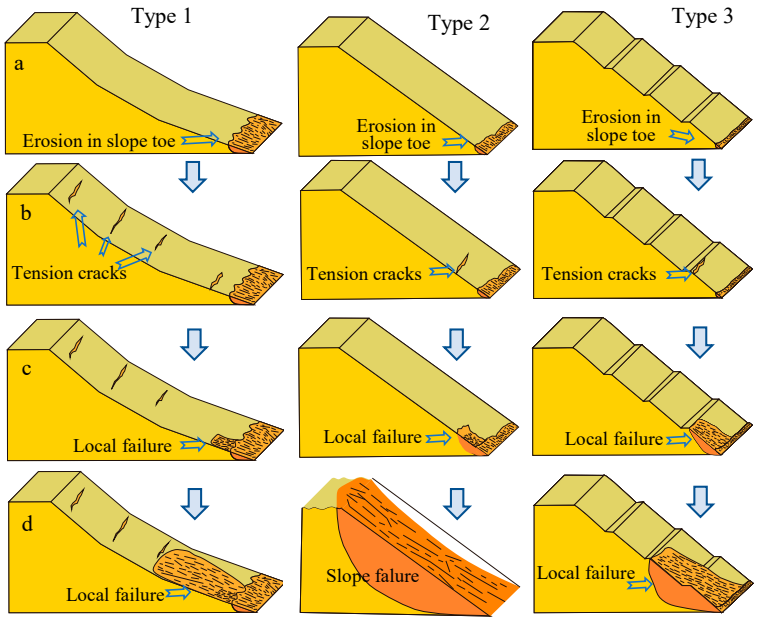

Figure 8. Failure models of different slope failures triggered by rainfall ((**a**–**d**) are the following stages and Type 1, 2 and 3 are the different protective measures of slopes).

4. Discussion

The slopes of the three types of mitigation measures all underwent toe erosion, and formation and expansion of local failures, but the degree of slope changes at each stage were not the same. During the toe erosion stage, the main erosion and damage location of the three types of slopes were all concentrated at the toe. However, the slope with a declining gradient mitigation experienced the earliest erosion damage as well as the largest erosion at the toe. The step-by-step and drainage canal mitigation slope had the least amount of slope erosion (Figure 9). During the local failure stage, the slope without any mitigation measures formed steep lateral free faces after local failures, and the slope with a declining gradient mitigation collapsed rather than sliding; it experienced relatively little deformation. Furthermore, high and steep lateral free faces did not appear in the toe of the slope with slope down the slope step-by-step mitigation after local failure. The slope with a stepwise drainage channel mitigation was more prone to local failure and had deeper sliding surfaces due to the settlement cracks that occurred near the drainage channels (Figure 10). In the later stage of the experiment, both the slope without any mitigation measures and the slope with a declining gradient mitigation exhibited local failures. When overall failure occurred, the sliding back edge of the slope without any mitigation measure was located at the top of the slope, and the sliding surface was deeper. The sliding back edge of the slope with a declining gradient mitigation was located in the middle part of the slope surface, and the failure was shallow, with a thin sliding surface (Figure 11).

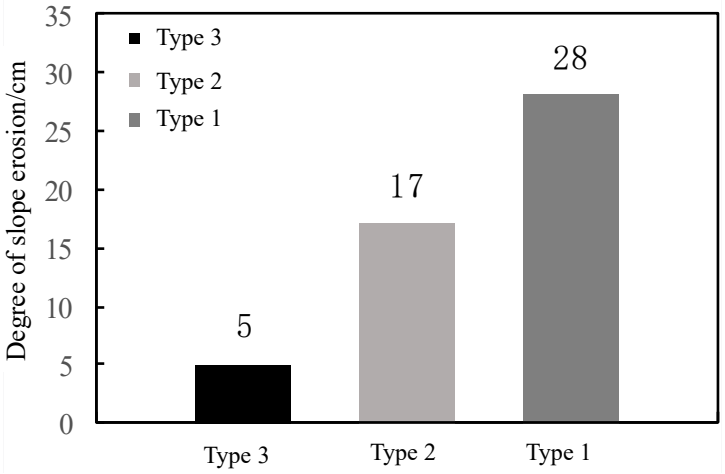

Figure 9. Erosion in the slope toe of different slopes.

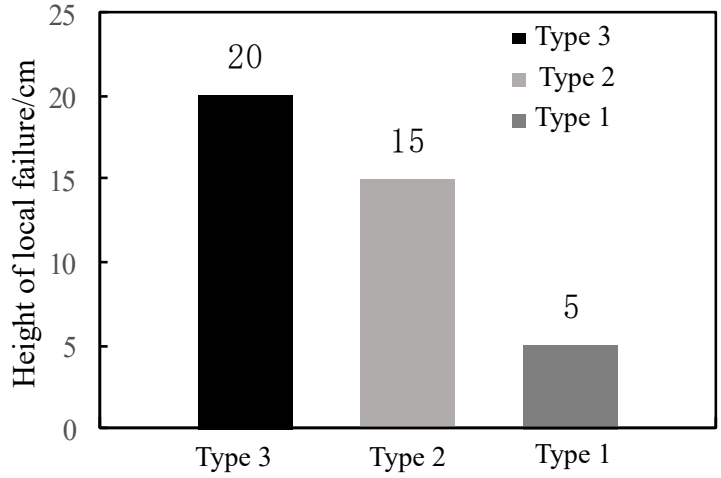

Figure 10. Heights of local failures of different slopes.

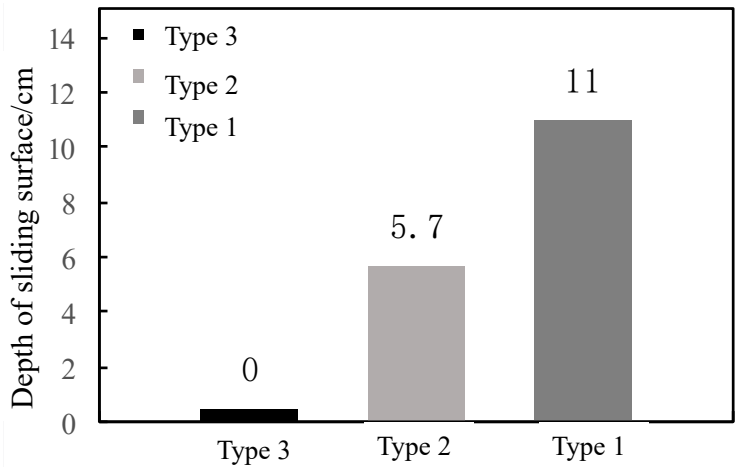

Figure 11. Depth of sliding surfaces of different slopes.

Based on the displacement data and observed experimental phenomena, we found the creep process of slopes with different mitigation measures to be different. During the experiment, tensile cracks appeared on all three types of slopes, and the appearance of tensile cracks on the slope without any mitigation measure had a clear chronological order. Tensile cracks first appeared at the toe of this slope, followed by a local failure at the toe of the slope. Tensile cracks then appeared at the middle and then the upper part of the slope. In contrast, the slope with a declining gradient mitigation had tensile cracks appearing simultaneously at different positions on the slope surface, with no clear chronological order. This indicates that the creep of the slope with a declining gradient mitigation occurred simultaneously at the toe, middle, and upper part of the slope, thus causing tensile cracks to appear at these positions simultaneously. The slope with a stepwise drainage channel mitigation had tensile cracks near the transverse drainage channels on the slope surface. For the slope without any mitigation measures, due to the influence of the erosion at the toe of the slope, the lateral stress at the toe of the slope was greater than at the bottom, and therefore the creep was more obvious at the toe of the slope [45,46]. As a result, tensile cracks appeared at the toe of the slope first, followed by the middle and upper parts as a consequence of local failures. The slope with a stepwise drainage channel mitigation experienced discontinuous creep, and cracks were prone to occur near the drainage channels due to differences in deformation.

During the testing, slopes with different mitigation measures exhibited different characteristics in water infiltration and erosion, pore-water pressure, and slope deformation. However, there were also commonalities in the failure processes of all the slopes, such as erosion and failure at the toe of the slope being a prelude to subsequent slope failures. The toe of the slope is the most susceptible area to slope failure, so when carrying out slope protection, attention should be paid to protecting the toe of the slope to prevent failure caused by erosion. In addition, slopes with different types of protection also exhibited local failures induced by erosion in the surface of the slope. Therefore, filled slopes compaction alone is not enough to ensure their stability. The surface of the slope should also be treated with methods such as tree planting, anchoring, and gridding to improve its erosion resistance. Using a mitigation method of reducing the slope gradient can effectively improve the stability of a slope, reducing deformation under rainfall. However, long slope surfaces tend to exhibit a significant convergence flow effect, which may exacerbate the erosion in the toe of the slope [42,43,45,46,48].

Thus, for loess-filled slopes, slope mitigation should be combined with slope surface protection and drainage, and the slope erosion caused by water flow should be reduced by building lateral drainage channels. In terms of soil reinforcement, this can be achieved by chemical reinforcement, anchoring, and other means that can increase the strength of the soil in loess-filled slopes and prevent strength attenuation caused by rainfall infiltration [49,50].

In addition, a retaining wall should be set at the toe of a slope to prevent erosion damage and to ensure stability.

5. Conclusions

This study examined the instability process and mechanism of remolded loess slopes under heavy rainfall with different protective measures (without any mitigation measures, with a declining gradient mitigation, and with a stepwise drainage channel mitigation). Our conclusions are below.

1. Changes in water content and pore-water pressure inside the slope were mainly concentrated in the shallow part of the slope and in the range of 5 cm during rainfall. With continuous rainfall, when a slope failed locally, changes in soil water content and pore-water pressure on the slope without any mitigation measure were obvious, and the water content and pore-water pressure everywhere showed a sudden response to the failure. The other two slopes' water content and pore-water pressure responses were weaker.
2. The modes of failure of slopes with different protective measures were different. The slope without any mitigation measures was the most susceptible to erosion. Although the slope with a declining gradient mitigation was the least likely to experience overall failure and has relatively small local failures, the degree of erosion on the slope surface was more severe than with other mitigation measures. The use of the step-by-step and drainage canal mitigation measure effectively prevented slope surface flow convergence, reducing the scouring effect of rainfall on the slope surface, but this slope was prone to local sliding with its deeper surfaces along the transverse drainage canals ditch.
3. The pore-water pressure response and the development of tensile cracks in the slope soil affect the degree of deformation of the slope, and these are the driving factors behind the differences in the failure characteristics of slopes with different protective measures. So, it is an effective way that reduce the infiltration of rainfall to slope, prevent the deep cracks of the slope due to discontinuity deformation, and weaken the confluence of the slope to prevent the large deformation of the filled slope.

Author Contributions: Conceptualization, J.Z. and Y.Z. (Yi Zhu); methodology, J.Z. and Y.Z. (Yong Zhao); software, Y.Z. (Yi Zhu) and Y.Z. (Yong Zhao); investigation, Y.Z. (Yi Zhu), J.Z. and Y.Z. (Yong Zhao); data curation, Y.Z. (Yi Zhu), J.Z. and Y.Z. (Yong Zhao); writing—original draft preparation, Y.Z. (Yi Zhu) and Y.Z. (Yong Zhao); writing—review and editing, Y.Z. (Yi Zhu), J.Z. and Y.Z. (Yong Zhao); project administration, J.Z.; funding acquisition, J.Z. All authors have read and agreed to the published version of the manuscript.

Funding: This research was funded by the National Natural Science Foundation of China: 42090053, 41922054.

Data Availability Statement: The data presented in this study are available on request from the corresponding author.

Acknowledgments: The authors are very grateful to the anonymous reviewers and editors for their thoughtful review comments and suggestions which have significantly improved this paper.

Conflicts of Interest: The authors declare no conflict of interest.

References

1. Liu, T.S. *Loess and the Environment*; Science Press: Beijing, China, 1985.
2. Li, Y.R.; Shi, W.; Aydin, A.; Beroya-Eitnerc, M.A.; Gao, G.H. Loess genesis and worldwide distribution. *Earth-Sci. Rev.* **2020**, *201*, 1–99. [CrossRef]
3. Zhuang, J.Q.; Peng, J.B.; Wang, G.H.; Javed, I.; Wang, Y.; Li, W. Distribution and characteristics of landslide in Loess Plateau A case study in Shaanxi province. *Eng. Geol.* **2017**, *236*, 89–96. [CrossRef]
4. Derbyshire, E.; Meng, X.M.; Dijkstr, T.A. *Landslides in the Thick Loess Terrain of North-West China*; John Wiley: Hoboken, NJ, USA, 2001; Volume 59, pp. 201–202.

5. Fu, B.; Liu, Y.; Lü, Y.; He, C.; Zeng, Y.; Wu, B. Assessing the soil erosion control service of ecosystems change in the Loess Plateau of China. *Ecol. Complex.* **2011**, *8*, 284–293. [CrossRef]
6. Duan, Z.; Zhang, H.; Tao, H.; Ma, J.Q.; Wu, S.Y. Mechanism of erosion induced landslide in Loess Plateau area in the Lower Reaches of Jing River. *Geol. Sci. Technol. Inf.* **2023**, *38*, 10–16.
7. Feng, L.; Lin, H.; Zhang, M.S.; Guo, L.; Jin, Z.; Liu, X. Development and evolution of Loess vertical joints on the Chinese Loess Plateau at different spatiotemporal scales. *Eng. Geol.* **2020**, *265*, 105372. [CrossRef]
8. Liu, G.; Zheng, F.; Wilson, G.V.; Xu, X.; Liu, C. Three decades of ephemeral gully erosion studies. *Soil Till. Res.* **2021**, *212*, 105046. [CrossRef]
9. Wang, G.L.; Li, T.L.; Xing, X.L.; Zou, Y. Research on loess flow-slides induced by rainfall in July 2013 in Yan'an, NW China. *Environ. Earth Sci.* **2015**, *73*, 7933–7944. [CrossRef]
10. Zhuang, J.Q.; Ma, P.H.; Zhan, J.W.; Zhu, Y.; Kong, J.X.; Zhu, X.H.; Leng, Y.Q.; Peng, J.B. Empirical relationships of the landslides in the Chinese Loess Plateau and affect factors analysis. *Geomat. Nat. Hazards Risk* **2022**, *13*, 250–266. [CrossRef]
11. Li, P.Y.; Qian, H.; Wu, J.H. Accelerate research on land creation. *Nature* **2014**, *7503*, 29–31. [CrossRef]
12. Juang, C.H.; Dijkstra, T.; Wasowski, J.; Meng, X.M. Loess geohazards research in china: Advances and challenges for mega engineering projects. *Eng. Geol.* **2019**, *251*, 1–10. [CrossRef]
13. Bao, H.; Tang, M.; Lan, H.X.; Peng, J.B.; Zheng, H.; Guo, G.M. Soil erosion and its causes in high-filling body: A case study of a valley area on the Loess Plateau, China. *J. Mt. Sci.* **2023**, *20*, 182–196. [CrossRef]
14. Tang, J.; Sui, L.; Ma, T.; Dan, Y.; Yang, Q.; Zhao, R.; Qiang, X. GEE-Based Ecological Environment Variation Analysis under Human Projects in Typical China Loess Plateau Region. *Appl. Sci.* **2023**, *13*, 4663. [CrossRef]
15. Zhu, Y.; Zhuang, J.Q.; Zhao, Y. Evaluation of loess-filled slope failure triggered by groundwater rise using a flume test. *Geomat. Nat. Hazards Risk* **2022**, *13*, 2471–2488. [CrossRef]
16. Cevasco, A.; Brandolini, P.; Scopesi, C.; Rellini, I. Relationships between geo-hydrological processes induced by heavy rainfall and land-use: The case of 25 October 2011 in the Vernazza catchment (Cinque Terre, NW Italy). *J. Maps* **2013**, *9*, 289–298. [CrossRef]
17. Guo, W.; Luo, L.; Wang, W.; Liu, Z.; Chen, Z.; Kang, H.; Yang, B. Sensitivity of rainstorm-triggered shallow mass movements on gully slopes to topographical factors on the Chinese Loess Plateau. *Geomorphology* **2019**, *337*, 69–78. [CrossRef]
18. Leonarduzzi, E.; Brian McArdell, W.; Molnar, P. Rainfall-induced shallow landslides and soil wetness: Comparison of physically based and probabilistic predictions. *Hydrol. Earth Syst. Sci.* **2021**, *25*, 5937–5950. [CrossRef]
19. Lu, N.; Godt, J.W. *Hillslope Hydrology and Stability*; Cambridge University Press: Cambridge, UK, 2013.
20. Toll, D.G.; Lourenco, S.D.N.; Mendes, J.; Gallipoli, D.; Evans, F.D.; Augarde, C.E.; Tang, A.M.; Vidovic, J.C.R.; Pagano, L.; Mancuso, C.; et al. Soil suction monitoring for landslides and slopes. *Q. J. Eng. Geol. Hydrogeol.* **2011**, *44*, 23–33. [CrossRef]
21. Xu, L.; Dai, F.C.; Tu, X.B.; Tham, L.G.; Zhou, Y.F.; Javed, I. Landslides in a loess platform, North-West China. *Landslides* **2014**, *11*, 993–1005. [CrossRef]
22. Peng, J.B.; Zhang, F.Y.; Wang, G.H. Rapid loess flow slides in Heifangtai terrace, Gansu, China. *Q. J. Eng. Geol. Hydrogeol.* **2017**, *50*, 106–110. [CrossRef]
23. Qi, X.; Xu, Q.; Zhu, X.; Peng, D.L.; Ju, Y.Z.; Li, H.J. Deformation characteristics and formation mechanism of static liquefaction No.8 loess landslide in Chenjia, Heifangtai, Gansu Province. *Geol. Sci. Technol. Inf.* **2018**, *37*, 234–239.
24. Qiu, H.J.; Hu, S.; Wang, X.G.; Yang, D.D.; Pei, Y.Q. Size and spatial distribution of loess slides on the chinese loess plateau. *Phys. Geogr.* **2020**, *41*, 126–144. [CrossRef]
25. Yin, Y.; Li, B.; Wang, W.; Zhan, L.; Xue, Q.; Gao, Y.; Zhang, N.; Chen, H.; Liu, T.; Li, A. Mechanism of the December 2015 catastrophic landslide at the Shenzhen landfill and controlling geotechnical risks of urbanization. *Engineering* **2016**, *2*, 230–249. [CrossRef]
26. Wang, J.; Xu, Y.; Ma, Y.; Qiao, S.N.; Feng, K.Q. Study on the deformation and failure modes of filling slope in loess filling engineering: A case study at a loess mountain airport. *Landslides* **2018**, *15*, 2423–2435. [CrossRef]
27. Zhan, L.; Zhang, Z.; Chen, Y.; Cen, R.; Zhang, S.; Liu, J.; Li, A.G. The 2015 Shenzhen catastrophic landslide in a construction waste dump: Reconstitution of dump structure and failure mechanisms via geotechnical investigations. *Eng. Geol.* **2018**, *238*, 15–26. [CrossRef]
28. Wang, G.; Sassa, K. Factors affecting rainfall-induced flowslides in laboratory flume tests. *Geotechnique* **2001**, *51*, 587–599. [CrossRef]
29. Bian, X.C.; Jiang, H.G.; Cheng, C.; Chen, Y.M.; Chen, R.P.; Jiang, J.Q. Full-scale model testing on a ballastless high-speed railway under simulated train moving loads. *Soil Dyn. Earthq. Eng.* **2014**, *66*, 368–384. [CrossRef]
30. Zhang, H.; Yang, J.; Wang, L.; Xu, Y.F. Model test on the dynamic characteristics of crack formation in expansive soil slopes under alternate drying and wetting. *Acta Geotech.* **2023**, *18*, 2097–2115. [CrossRef]
31. Schnellmann, R.; Busslinger, M.; Schneider, H.R.; Rahardjo, H. Effect of rising water table in an unsaturated slope. *Eng. Geol.* **2010**, *114*, 71–83. [CrossRef]
32. Li, X.; Niu, J.; Li, J.; Xie, B.Y.; Han, Y.N.; Tan, J.P.; Zhang, Y.H. Characteristics of runoff and sediment generation of forest vegetation on a hill slope by use of artificial rainfall apparatus. *J. For. Res.* **2012**, *23*, 419–424. [CrossRef]
33. Zhang, X.; Yu, G.Q.; Li, Z.B.; Li, P. Experimental study on slope runoff, erosion and sediment under different vegetation types. *Water Resour. Manag.* **2014**, *28*, 2415–2433. [CrossRef]

34. Wu, L.Z.; Zhou, Y.; Sun, P.; Shi, J.S.; Liu, G.G.; Bai, L.Y. Laboratory characterization of rainfall-induced loess slope failure. *Catena* **2017**, *150*, 1–8. [CrossRef]
35. Lin, H.Z.; Yu, Y.Z.; Li, G.X.; Peng, J.B. Influence of rainfall characteristics on soil slope failure. *Chin. J. Rock Mech. Eng.* **2009**, *28*, 198–204.
36. Rolando, P.O.; Suquru, S.; Kenqo, M.; Ikuo, T. Instrumented model slope failure due to water seepage. *J. Nat. Disaster Sci.* **2004**, *26*, 15–26.
37. Ahmadi-Adli, M.; Huvaj, N.; Toker, N.K. Rainfall-triggered landslides in an unsaturated soil: A laboratory flume study. *Environ. Earth Sci.* **2017**, *76*, 735. [CrossRef]
38. Hu, W.; Xu, Q.; Rui, C.; Huang, R.Q.; van Asch, T.W.J.; Zhu, X.; Xu, Q.Q. An instrumented flume to investigate the initiation mechanism of the post-earthquake huge debris flow in the southwest of China. *Bull. Eng. Geol. Environ.* **2015**, *74*, 393–404. [CrossRef]
39. Hu, W.; Dong, X.J.; Xu, Q.; Wang, G.H.; van Asch, T.W.J.; Hicher, P.Y. Initiation processes for run-off generated debris flows in the Wenchuan earthquake area of China. *Geomorphology* **2016**, *253*, 468–477. [CrossRef]
40. Hu, W.; Xu, Q.; Wang, G.H.; van Asch, T.W.J.; Hicher, P.Y. Sensitivity of the initiation of debris flow to initial soil moisture. *Landslides* **2015**, *12*, 1139–1145. [CrossRef]
41. Wang, G.; Sassa, K. Pore-pressure generation and movement of rainfall-induced landslides: Effects of grain size and fine-particle content. *Eng. Geol.* **2003**, *69*, 109–125. [CrossRef]
42. Huang, X.J.; Horn, R.; Ren, T.S. Soil structure effects on deformation, pore water pressure, and consequences for air permeability during compaction and subsequent shearing. *Geoderma* **2022**, *406*, 115452. [CrossRef]
43. Hu, J.T.; Zhang, H.; Li, Z.; Yang, S.Q.; Zhang, S.R.; Li, H.C.; Lu, M. Study on pore-water pressure variation and deformation characteristics of warm frozen soils under confined dynamic loading. *Cold Reg. Sci. Technol.* **2023**, *214*, 103968. [CrossRef]
44. Tokimatsu, K.; Suzuki, H. Pore Water Pressure Response Around Pile and its Effects on P-Y behavior During Soil Liquefaction. *Soils Found.* **2004**, *44*, 101–110. [CrossRef] [PubMed]
45. Xiu, Z.; Wang, S.; Ji, Y.; Ji, Y.C.; Wang, F.L.; Ren, F.Y. Experimental investigation on liquefaction and post-liquefaction deformation of stratified saturated sand under cyclic loading. *Bull. Eng. Geol. Environ.* **2020**, *79*, 2313–2324. [CrossRef]
46. Niu, L.; Hu, X.; Xu, C.; Wang, J.; Li, Y.B.; Zhang, H.H. Physical model test of the deformation mechanism of the multi-sliding zones landslide subjected to the operated reservoir. *Bull. Eng. Geol. Environ.* **2023**, *82*, 213. [CrossRef]
47. Liu, H.D.; Liu, J.J.; Chen, J.X.; Guo, Z.F.; Qiu, L. Experimental study on tilting deformation and a new method for landslide prediction with retaining-wall locked segment. *Sci. Rep.* **2023**, *13*, 5149. [CrossRef] [PubMed]
48. Wu, Y.; Lu, G.; Zhu, Z.; Bai, D.; Zhu, X.; Tao, C.; Li, Y. A Landslide Warning Method Based on K-Means-ResNet Fast Classification Model. *Appl. Sci.* **2023**, *13*, 459. [CrossRef]
49. Mu, J.; Zhuang, J.; Kong, J.; Wang, S.; Wang, J.; Zheng, J.; Fu, Y.; Du, C. Study on Improving Loess Properties with Permeable Polymer Materials. *Polymers* **2022**, *14*, 2862. [CrossRef]
50. Chen, C.K.; Li, G.; Liu, J.; Nan, J.J. Shear strength characteristics of basalt fiber-reinforced loess. *Sci. Rep.* **2023**, *13*, 15923. [CrossRef]